# Radiative Flow and Heat Transfer of Chemically Reacted Casson Nanofluid Over a Wedge Under the Influence of MHD and Viscous Dissipation

KAVITHA G.[1], VITTAL CH.[2], VIJAYALAXMI TANKASALA [3, *], DHANALAXMI V. [1]

[1.] Department of Mathematics, Osmania University, Hyderabad-500007, Telangana, INDIA.
[2.] Department of Mathematics, University College of Science, Saifabad, Osmania University, Hyderabad-500007, Telangana, INDIA.
[3.] Department of Mathematics, NTR Govt. Degree & P.G. College for Women, Mahabubnagar-509001, Telangana, INDIA.
* Corresponding author email: vijaya9966998024@rediffmail.com

*Abstract:* The effect of thermal radiation, viscous dissipation with magnetohydrodynamic and chemically reacted Casson Nano fluid flow across a moving wedge and convective boundary condition in existence of internal heat generation/absorption is studied, the obtained results are presented. The simple governing partial differential equations are altered into non-linear ordinary differential equations through employing suitable similarity transformations. The obtained non-linear ordinary differential equations are effectively elucidated numerically through Keller-Box method by use of MATLAB software. The variation of the pertinent constraints on velocity, temperature and nanoparticle volume fraction are explored through graphs. The graphs of skin friction coefficient, Nussult number and Sherwood number are plotted as a function of physical parameters for different values. The present results are well matched with the previous reported work. The present work demonstrates the nanoparticle volume fraction profile decrease by enhance of chemical reaction, Brownian motion, Schmidt parameter values and increases with increment in thermophoresis parameter values.

*Key-words*: Nanoparticle, Thermophoresis, Brownian motion, Schmidt number, Chemical reaction, Wedge.

Received: March 14, 2024. Revised: August 7, 2024. Accepted: September 9, 2024. Published: October 17, 2024.

## 1. Introduction

Non-Newtonian fluids attracted many researchers, scientists and engineers due to its wide range of applications in industry, manufacturing processing, biological fluids etc. Due to many potential and technological applications, the non-Newtonian fluids are considered the most important than viscous fluids. Non-Newtonian fluids exhibits variable viscosity as a result of applied force. To analyze the behavior of non-Newtonian liquids, numerous significant difficulties are encountered, comprises highly nonlinear governing boundary layer equations and a higher degree of complexity than Newtonian fluids. Hence, few reports are available [1-7] and need further investigation for better understanding of the flow characteristics of non-Newtonian fluids. Casson fluid model is one of the simplest, non-Newtonian fluid model of differential type. The reported studies revealed the Casson fluid model is fit to the rheological data and it is better than general viscoplastic models for many materials. Casson fluid exhibits a yield stress. The Casson model is accurate in very low and very high shear rate. This model is used in industries to get more accurate representation of high shear rate viscosities when only low and intermediate shear rate data are available. Besides, Casson fluids witnessed significant applications in polymer processing industries and biomechanics. Recently, many researchers are

considered the boundary layer flow of Casson fluid over dissimilar geometries. Studies on magnetohydrodynamics (MHD) flow of a Casson fluid over an exponentially shrinking sheet has made by Nadeem et al. [8]. The reported literature available on flow analysis of Casson fluids is made by Hayat et al. [9], Bhattacharyya et al. [10], and Mukhopadhyay et al. [11], Nadeem et al. [12], Haq et al. [13].

The convective flow past a wedge has been widely studied by researchers due to its applications in aerodynamics, heat exchangers, geothermal systems, etc. Furthermore, the wedge flow is important due to the fact that each value of wedge angle yields a diverse pressure profile, thereby offer insight into boundary layer behavior in number of situations. The Falkner-Skan (F-S) wedge flow for a non-Newtonian fluid with a variable free stream condition is reported by Postelnicu and Pop [14]. Kafoussias group [15] explored the MHD laminar boundary-layer flow of a non-Newtonian fluid over a permeable wedge. Swati Mukhopadhyay and group members [16] examined the boundary layer forced convection flow of a Casson fluid past a symmetric wedge. The observed results demonstrates rise of the Casson fluid parameter, the fluid velocity increases and the temperature decreased. The fluid velocity is suppressed with the increase of suction. Kishan et al. studied the magnetohydrodynamic heat transfer of non-Newtonian power-law fluids flowing over a wedge [17, 18]. Wedge flow analysis at different thermophysical conditions is reported by many researchers [19-23]. Su et al. demonstrate an MHD mixed convection flow of viscous fluid via a porous stretching wedge [24]. Hossain et al. reported the flow of an unsteady mixed-convection boundary layer through a symmetric wedge with a changing surface temperature [25]. Deka and Sharma examined the magnetohydrodynamic mixed convection flow through a wedge with changing temperature and chemical reaction using Falkner-Skan transformations [26]. Srinivasacharya et al. investigated heat, mass transport characteristics are stable in a laminar MHD flow across a wedge in the presence of changing magnetic fields [27].

Hall effects on MHD squeezing flow of a water based nanofluid through a saturated porous medium in between two parallel disks is studied as consider the Hall current into the account by Veera Krishna et al [28]. Study on effects of heat, mass transfer on free convective flow of micropolar fluid over an infinite vertical porous plate in presence of inclined magnetic field with an angle of inclination, constant suction velocity by Veera Krishna and team members [29]. Recent studies on the effects of various non-dimensional parameters on velocity, temperature and concentration within the boundary layer are examined through Soret and Joule effects with MHD mixed convective flow of an incompressible, electrically conducting viscous fluid past an infinite vertical porous plate, the Perturbation technique is used to solve the non-dimensional equations [30]. Hall and ion slip effects on magnetohydrodynamic (MHD) free convective rotating flow of nanofluids in a porous medium past a moving vertical semi-infinite flat plate are investigated by Chamkha et al in the year 2020, and found the impact of thermal convection of nanoparticles has increased the temperature distribution, which helps in destroying the cancer cells during the drug delivery process [31]. Chamkha and team studied the effect of MHD flow of an electrically conducting second-grade fluid through porous medium over a semi-infinite vertical stretching sheet by consider the thermophoresis, thermal radiation, and convective boundary conditions. The fluid velocity, temperature in the boundary layer area become considerably higher with enhance the values of the thermal radiation parameter. The Nusselt number is improved by increase of surface convection parameter [32]. Heat transfer on the peristaltic magnetohydrodynamic flow of a Jeffrey fluid through a porous medium in a vertical echelon under the influence of a uniform transverse magnetic field normal to the channel

and its effect by consider the Hall current into account is made by Chamkha team in the year 2018. The size of the trapping bolus decreases by enhance in Hartmann number or permeability parameter and raises with increase of Hall parameter or Jeffrey number [33].

Recently, cooling of electronic devices, gadgets, etc. is the major industrial requirement. Due to the lower thermal conductivity rate of ordinary base fluids like water, ethylene glycol, oil, etc. the nanoscale solid particles are mixed with the fluids which results in vary the thermophysical characteristics of these fluids and improved heat transfer rate dramatically. In the year 1996 the first report on the nature of the colloidal suspension, studied by Choi and team members [34]. Recently, advancement of nanofluids, its mathematical modelling, etc. plays a vital role in industrial and nanotechnology. Nanofluids are used in various applications like cooling of electronics devices / industry, nuclear reactor safety, heat ex-changer, biomedicine, hyperthermia, vehicle thermal management, engine cooling, many others. Two mechanisms have been processed to elucidate the increase effective thermal conductivity in nanofluids, one is due higher thermal conductivity of the nanoparticles and second one is contribution from the Brownian motion of the nanoparticles. The implication of the two contributions is closely associated to the bulk temperature of the nanoparticle's suspension, the size and the volume fraction of the nanoparticles in the nanofluid, as well as the thermophysical properties of the nanoparticles and the base fluid materials. Many researchers in fluid dynamics are extended an interest in nanofluids over the last few years owing to its potential applications. It directed the mixing of fluids with metal nanoparticles towards improve the heat transfer capacity of the fluids. Brownian motion of nanoparticles at molecular and nanoscale levels is an important nanoscale mechanism governing its thermal behavior. In nanofluid, due to its size of the nanoparticles, the Brownian motion takes place, which could influence the heat transfer properties. Brownian motion aids to warm the boundary layer and simultaneously aggravates particle deposition away from the fluid regime, thereby accounting for the reduced concentration magnitudes. Choi and team members [35] studied addition of small amount of nanoparticles to the base fluid which results in increased thermal conductivity. Investigation on boundary layer flow of Casson nanofluid over a vertical exponentially stretching cylinder is made by Malik et al. [36]. Haq et al., reported on heat transfer and MHD effects on Casson nanofluid flow over a shrinking sheet, results show the trend of velocity is identical for MHD, Casson fluid and shrinking parameters [37]. Studies on MHD mixed convection stagnation-point flow of a non-Newtonian power-law nanofluid for a stretching surface is done by Madhu and Kishan, results states the effect of magnetic field parameter reduces the velocity profiles [38]. Mustafa examined the MHD flow of Casson nanofluid past a non-linearly stretching, the observations states the velocity decreases and skin friction coefficient increases as strength of magnetic field is increased. The velocity, boundary layer thickness decreased with the Casson fluid parameter, Skin friction coefficient for Casson fluid is greater than that for Newtonian fluid [39]. The effect of slip, convective boundary condition on magneto-hydrodynamic stagnation point flow and heat transfer due to Casson nanofluid past a stretching sheet is reported by Ibrahim and Makinde [40]. Chamkha et al. observed the influence of radiation on mixed convection in the presence of a wedge implanted in a porous media filled with a nanofluid, the observed results are very good agreement with the reported results. It is found that the local Nusselt number increases when any of the buoyancy ratio, the Brownian motion, the thermophoresis, the radiation–conduction and the surface temperature parameters, and the Lewis number increases. Whereas the local Sherwood number is increased as the buoyancy ratio, Brownian motion parameter, Lewis number, wedge angle parameter, radiation–conduction parameter or the surface temperature parameter

increases [41]. Boundary layer flow through a moving wedge in a nanofluid is explored by Khan and Pop, found that the dimensionless velocity at the surface increases / decreases with stretching / shrinking parameters, and dimensionless temperature increases with both Brownian motion and thermophoresis parameters [42]. Mahdy team studied on unsteady MHD boundary layer flow of a moving stretched porous wedge containing tangent hyperbolic two phase nanofluid [43]. Studies on heat and mass transfer nature of Casson nanofluid flow over a moving wedge filed is made by Amar and Kishan [44], and concluded that the flow velocity increases with enhance in wedge angle and the thickness of the boundary layer is decline with increase of magnetic field parameter in wedge positions. The flow velocity is decrease with increase of Casson parameter and permeability parameter, whereas the skin friction coefficient enhances with increase of magnetic field parameter. Jamal Shah and team studied the MHD flow of Casson nanofluid for the applications of gold nanoparticles flow [45], the results conclude that increase of the volume percentage of gold nanoparticles from 0 to 0.04 percent towards an increase of up to 3.825 % in the heat transfer rate. Recently, investigation of the three-dimensional Casson hybrid nanofluid (ZnO + Ag) flow under the influence of an applied changing magnetic flux is reported, results show the hybrid nanofluid performed excellent transfer of heat, could use for cooling purposes of the system [46]. Chamkha group investigated the dissipative MHD free convective nanofluid flow past a vertical cone under radiative chemical reaction with mass flux studies [47]. The flow, heat and mass transfer nature of Casson nanofluid past an exponentially stretching surface with activation energy, Hall current, thermal radiation, heat source/sink, Brownian motion and thermophoresis studies are made by Suresh Kumar group [48].

To the best of author's knowledge, no reports are available in the literature on the Casson nanofluid flow over a wedge under the influence of chemical reaction with magnetic field effect. In the present study, investigation on chemical reaction influence, flow and heat transfer characteristics of a Casson nanofluid on a wedge under the influence of uniform transverse magnetic field is made, the observed results are presented. The effects of the various flow controlling parameters on velocity, temperature and nanoparticle volume fraction have been investigated numerically and analysed with the help of their graphical representations.

## 2. Model description

The present work is formulated as mentioned below.

- Consider the two - dimensional steady incompressible flow and MHD heat transfer of a chemically reacted Casson nanofluid over a moving wedge in the occurrence viscous and radiation effect.
- The induced magnetic field is ignored due to applied magnetic field is very high.
- The moving wedge surface maintains constant temperature due to convective heat transfer and the lower surface of the wedge heated by convection from a hot fluid at temperature $Tf$ with heat transfer quantity $h_f$.
- A wedge surface is extending with a constant velocity $U_w(x)$ is subject to the laminar boundary layer that is indicated by $U_w(x) = ax^m$.
- When $U_w(x)$ positive that is the direction of the extending wedge is in the identical way to the fluid flow, while it negative indicates the shrinking wedge is in the reverse direction.
- The $U(x) = cx^m$ here $a, c$ $and$ $m$ are fixed as shown in the figure.

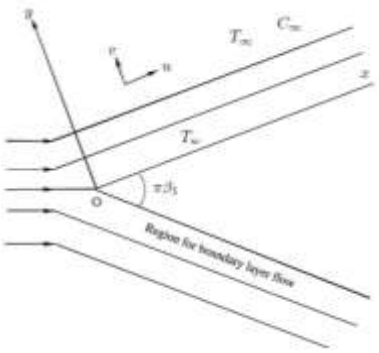


Figure 1: Flow configuration and co-ordinate system.

Based on N. Amar et al [49] & M. Madhu et al [50] the governing equations for above assumptions can be stated as

Continuity Equation is

$$\frac{\partial u}{\partial x}+\frac{\partial v}{\partial y}=0 \qquad (1)$$

Momentum Equation

$$u\frac{\partial u}{\partial x}+v\frac{\partial u}{\partial y}=-\frac{1}{\rho}\frac{dp}{dx}+\upsilon\left(1+\frac{1}{\gamma}\right)\frac{\partial^2 u}{\partial y^2}+\left(\frac{\sigma B_0^2(x)}{\rho}\right)(U(x)-u) \qquad (2)$$

Equation of Thermal Energy

$$u\frac{\partial T}{\partial x}+v\frac{\partial T}{\partial y}=\alpha\frac{\partial^2 T}{\partial y^2}+\frac{\vartheta}{\rho c_p}\left(\frac{\partial u}{\partial y}\right)^2+\frac{Q_0}{\rho C_p}(T-T_\infty)-\frac{1}{\rho C_p}\left(\frac{\partial q_r}{\partial y}\right) \qquad (3)$$

Equation of Species Concentration

$$u\frac{\partial C}{\partial x}+v\frac{\partial C}{\partial y}=D_B\frac{\partial^2 C}{\partial y^2}+\frac{D_T}{T_\infty}\frac{\partial^2 T}{\partial y^2}-K_0(C-C_\infty) \qquad (4)$$

The associated boundary conditions are

$$u=U\frac{df}{d\eta}=cx^m f'(\eta)x,\quad v=v_w(x)=v_0\sqrt{x^{m-1}},\quad -k\frac{\partial T}{\partial y}=h_f\left(T_f-T_w\right),\quad D_B\frac{\partial C}{\partial y}+\frac{D_T}{T_\infty}\left(\frac{\partial T}{\partial y}\right)=0 \ at\ y=0 \qquad (5)$$

$$u\to U(x),\quad T\to T_\infty,\quad C\to C_\infty,\quad as\quad y\to\infty \qquad (6)$$

Where $u$ and $v$ denotes the velocities in the direction of $x$-and $y$-respectively, $\gamma$ is the Casson fluid parameter, $\upsilon$ is the kinematic viscosity, $\rho_f$ is the density of the base fluid, $\sigma$ is the electrical conductivity, $\alpha$ is the thermal diffusivity, $(\rho c)_p$ is the effective heat capacity of the Nano particles, $(\rho c)_f$ is the heat capacity of the base fluid, $\tau=\frac{(\rho c)_p}{(\rho c)_f}$ is the ratio of the Nano particle heat capacity and base fluid heat capacity, $D_B$ is the Brownian motion diffusion coefficient and $D_T$ is the thermophoresis diffusion coefficient, $K_o(x)=\frac{k}{a(C_w-C_\infty)}$ is the chemical reaction parameter, with rate constant $K_o$, where $K_o>0$ for destructive reaction, $K_o<0$ for generative reaction and $K_o=0$ for no reaction. We consider that the magnetic field $B(x)=B_0(x)$, where the constant magnetic field is $B_0$.

Using the Rosseland [51] approximation the radiative heat flux is simplified as:

$$q_r=-\frac{4\sigma_i}{3K^*}\frac{\partial T^4}{\partial y} \cdots\cdots\cdots\cdots (7)$$

We assume that the temperature differences within the flow region, namely, the term $T^4$can be expressed as a linear function of temperature. The best linear approximation of $T^4$ is obtained by expanding it in a Taylor series about $T_\infty$ is

$$T^4=T_\infty^4+4T_\infty^3(T-T_\infty)+6T_\infty^2(T-T_\infty)^2+\cdots\cdots\cdots\cdots (8)$$

Neglecting higher order terms of $(T-T_\infty)$ from equation (8) and attained as

$$T^4\cong 4TT_\infty^3-3T_\infty^3 \cdots\cdots\cdots\cdots (9)$$

Using equation (9) into equation (7) we get

$$q_r=-\frac{16\sigma_i T_\infty^3}{3K^*}\frac{\partial T}{\partial y} \cdots\cdots\cdots\cdots (10)$$

The modified equation of (3) by the assistance of equation (10) is

$$u\frac{\partial T}{\partial x}+v\frac{\partial T}{\partial y}=\alpha\frac{\partial^2 T}{\partial y^2}+\frac{\vartheta}{\rho c_p}\left(\frac{\partial u}{\partial y}\right)^2+\frac{Q_0}{\rho C_p}(T-T_\infty)+\frac{1}{\rho C_p}\left(\frac{16\sigma_i T_\infty^3}{3(\rho C_p)_f K^*}\frac{\partial^2 T}{\partial y^2}\right)\cdots\cdots\cdots\cdot(11)$$

The stream function $\psi(x,\ y)$ is defined as below and satisfied the equation (1)

$$u=\frac{\partial\psi}{\partial y}\text{ and }v=-\frac{\partial\psi}{\partial x}\cdots\cdots\cdots(12)$$

The desired conversions are described as

$$\eta=y\left(\frac{(m+1)U(x)}{2\vartheta x}\right)^{\left(\frac{1}{2}\right)},\quad \psi=\left(\frac{2\vartheta xU(x)}{(m+1)}\right)^{\left(\frac{1}{2}\right)}f(\eta),\quad \theta(\eta)=\frac{T-T_\theta}{T_f-T_\infty},\quad \emptyset(\eta)=\frac{C-C_\theta}{C_f-C_\infty}$$

$$u=U\frac{df}{d\eta},\quad v=-\left(\frac{(m+1)\vartheta U(x)}{2x}\right)^{\left(\frac{1}{2}\right)}\left[f(\eta)+\frac{(m-1)}{(m+1)}\eta\frac{df}{d\eta}\right],\quad R=\frac{4\sigma_i T_\infty^3}{3kK^*}\cdots\cdots\cdots(13)$$

By employing the similarity transfigurations and equation (12) the governing equations (2), (3), (4) reduced to the following ordinary differential equations along with the boundary conditions

$$\left(1+\frac{1}{\gamma}\right)f'''(\eta)+f(\eta)f''(\eta)+\beta\left(1-\left(f'(\eta)\right)^2\right)+M\left(f'(\eta)-1\right)=0\qquad(14)$$

$$\left(1+\frac{4R}{3}\right)\theta''(\eta)+\Pr f(\eta)\theta'(\eta)+\Pr Ec\left(f''(\eta)\right)^2+(2-\beta)\Pr Q\theta(\eta)=0$$

$$\phi''(\eta)+Scf(\eta)\phi'(\eta)+\frac{Nt}{Nb}\theta''(\eta)-Sc\Gamma\phi(\eta)=0\qquad(16)$$

$$f(0)=s,\quad f'(0)=\lambda,\quad \theta'(0)=-bi\left[1-\theta(0)\right],\quad Nb\phi'+Nt\theta'=0\quad at\ \eta=0$$

$$f'(\infty)=1,\quad \theta(\infty)=0,\quad \phi(\infty)=0\qquad at\ \eta\to\infty\qquad(17)$$

The involved physical parameters are Casson fluid parameter $\gamma$, wedge parameter $\beta$, Velocity Ratio Parameter $\lambda<0$ relates to flow in the reverse direction in outside flow, $\lambda>0$ relates to flow in the same direction on a permeable extending wedge wall, and $\lambda=0$ relates to a surface of a stationary wedge. Magnetic field $M$, $s<0$ is the suction and $s>0$ is the injection, Prandtl Number $Pr$, $Q$ is the heat source or sink parameter, $Ec$ is the Eckert number, R is the thermal radiation parameter, $bi$ is the thermal slip parameter, $Sc$ is the Schmidt number, Brownian number $Nb$ , Thermophoresis parameter $Nt$, $\Gamma$ is the Chemical reaction parameter.

The shear stress at the surface of wedge is intended as follows:

$$\tau_w=\mu\left(\frac{\partial u}{\partial y}\right)_{y=0}\Rightarrow\tau_w=\mu\left(\frac{U(x)}{\upsilon x}\right)^{\left(\frac{1}{2}\right)}\left(\frac{d^2 f}{d\eta^2}\right)_{\eta=0}$$

The physical quantity of major interest is the local skin-friction coefficient $(Cf)$, local Nusselt number $Nu_x$ and local Sherwood number $Sh_x$ in non-dimensional form is given by

$$Re_x^{\frac{1}{2}}C_{fx}=\left(1+\frac{1}{\beta}\right)f'''(0)$$

Where $\tau_w=\mu\left(\frac{\partial u}{\partial y}\right)\ at\ y=0$

$$Nu_x=\frac{xq_v}{\kappa(T_f-T_\infty)}\ \ Where\ q_v=-\kappa\left(\frac{\partial T}{\partial y}\right)_{y=0}$$

$$\Rightarrow Re_x^{-\frac{1}{2}} Nu_x = -\theta'(0)$$

$$Sh_x = \frac{q_m x}{D_B(C_w - C_\infty)} \; where \; q_m = -D_B\left(\frac{\partial C}{\partial y}\right)_{y=0}$$

$$\Rightarrow Re_x^{-\frac{1}{2}} Sh_x = -\phi'(0)$$

Where $Re_x = \frac{ax^2}{\upsilon}$ be the Reynolds number

## 3. Numerical scheme

- By adopting Keller-Box method and utilize of MATLAB software, the following set of steps are implemented to get the solutions.
- In order to solve and transform the system of higher ordinary differential equations (14) – (16) with their corresponding initial and boundary conditions (17), introduction of new independent variables of $p(\eta),\ q(\eta),\ \theta(\eta) = \upsilon(\eta),\ g(\eta),\ \varphi(\eta) = m(\eta)\ and\ n(\eta)$ are made and transformed into first order differential equations and also the boundary conditions are changed, as mentioned in below.

$$f' = p, p' = q, \upsilon' = g \; and \; m' = n$$

- Hence, the equations (14) to (16) and (17) could be written as

$$\left(1 + \frac{1}{\gamma}\right) q' + fq + \beta(1 - p^2) + M(p - 1) = 0$$

$$\left(1 + \frac{4R}{3}\right) g' + Prfg + PrEcq^2 + PrQ(2 - \beta)\upsilon = 0$$

$$n' + Scfn + \frac{Nt}{Nb} g' - Sc\Gamma m = 0$$

- The boundary conditions in equation (17) has been modified as

$$f(0) = s, \quad p(0) = \lambda, \quad g(0) = -bi\big(1 - \upsilon(0)\big), \quad Nbn(0) + Ntg(0)' = 0$$

$$p(\eta) \longrightarrow 1, \quad \upsilon(\eta) \longrightarrow 0, \quad m(\eta) \longrightarrow 0$$

- The resultant differential equations are first expressed in the form of finite difference and then linearized through Newton's technique.
- To find the solution, block tri-diagonal elimination procedure is used to set of linear equations which are arranged into the matrix form.
- To get the accuracy, the following appropriate initial guesses have been chosen.

$$f(\eta) = (s + \lambda - 1) + \eta + e^{-\eta}, \quad \theta(\eta) = \left(\frac{bi}{1 + bi}\right) e^{-\eta}, \quad \varphi(\eta) = \left(\frac{-Nt}{Nb}\right)\left(\frac{bi}{1 + bi}\right) e^{-\eta}$$

- The choices of the above initial guesses depend on the convergence criteria and transformed boundary conditions equation of (17). The step size 0.001 is used to obtain the numerical solution with suitable decimal place of accuracy as the criterion of convergence.

## 4. Results and discussion

In order to authorize the present numerical method and the obtained numerical results are confirmed with the results obtained by N. Amar et al [49]., Ahmad et al [52] and Ullah et al [53] in Table 1 and Table 2 denotes the compared results with Ahmad et al [52], Kuo [54] and N. Amar et al [49]. Comparisons are found in good with the outcomes.

Table 1: Deviations of $Cf\sqrt{R_x}$ for different values of $s$ and the other values are $Nb = Nt = Sc = \Gamma = Ec = Q = bi = \Pr = \lambda = R = 0$

| $s$ | Ahmad et al.[52] | Ullah et al. [53] | Amar et al. [49] | Present study |
|---|---|---|---|---|
| -1 | 0.75655 | 0.7566 | 0.756572 | 0.756434 |
| -0.5 | 0.96922 | 0.9692 | 0.969230 | 0.969021 |
| 0 | 1.23258 | 1.2326 | 1.232588 | 1.232865 |
| 0.5 | 1.54175 | 1.5418 | 1.541751 | 1.541754 |
| 1 | 1.88931 | 1.8893 | 1.889314 | 1.889314 |

Table 2: Deviations of $Cf\sqrt{R_x}$ for different values of $\beta$ and the other values are $Nb = Nt = Sc = \Gamma = Ec = Q = bi = \Pr = \lambda = R = 0$

| $\beta$ | Ahmad et al. [52] | Kuo et al. [54] | Amar et al. [49] | Present study |
|---|---|---|---|---|
| 0 | 0.46959 | 0.469600 | 0.469600 | 0.469594 |
| 0.1 | 0.58703 | 0.587889 | 0.587035 | 0.587123 |
| 0.3 | 0.77475 | 0.775524 | 0.774755 | 0.774755 |
| 0.5 | 0.92768 | 0.927905 | 0.927680 | 0.927685 |
| 1 | 1.23258 | 1.231289 | 1.232588 | 1.232589 |
| 1.6 | 1.52151 | 1.518488 | 1.521514 | 1.521518 |
| 2 | 1.68721 | 1.683095 | 1.687218 | 1.687215 |

In ordered to understand the mathematical model the computational results are presented graphically for velocity, temperature and Nano particle volume fraction profiles for different values of flow controlling parameters in Figures 2 to 15. The skin friction co-efficient $\left(1+\frac{1}{\beta}\right) f''(0)$, Nusselt number $-\theta'(0)$ and Sherwood number $-\varphi'(0)$ origin graphs are presented through Figures 16-18.

The Casson parameter $(\gamma)$ has an influence on the velocity and temperature fields depicted in Figures 2(a) and 2(b) and it is noticed that the increase of the Casson parameter $(\gamma)$ enhances the velocity and drops the temperature.

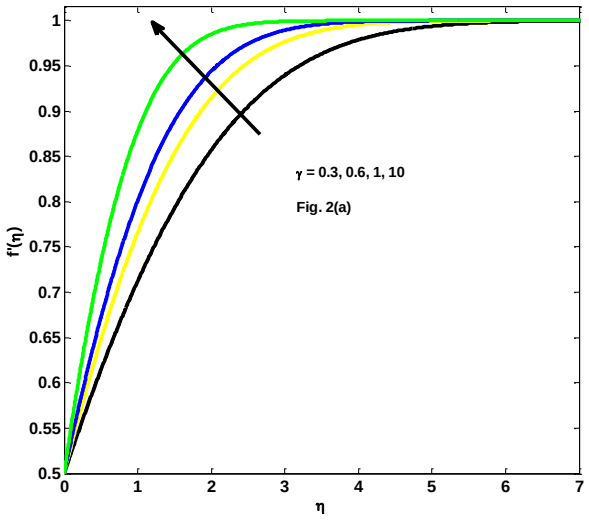


Figure 2(a): $f'(\eta)$ for picked values of $\gamma$

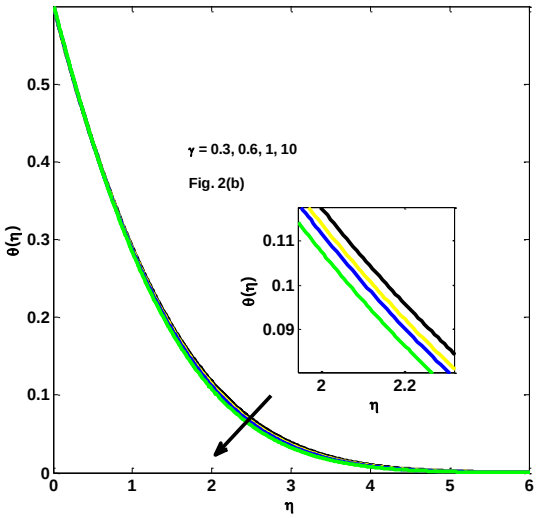


Figure 2(b): $\theta(\eta)$ for picked values of $\gamma$

The impact of changing the wedge parameter $(\beta)$ on the velocity and temperature are demonstrated in Figures 3(a) and 3(b). These figures exhibit that enhancing the wedge parameter values enriches the velocity and temperature profiles due to the pressure exerted on the flow, which accelerates the velocity area and the temperature profile.

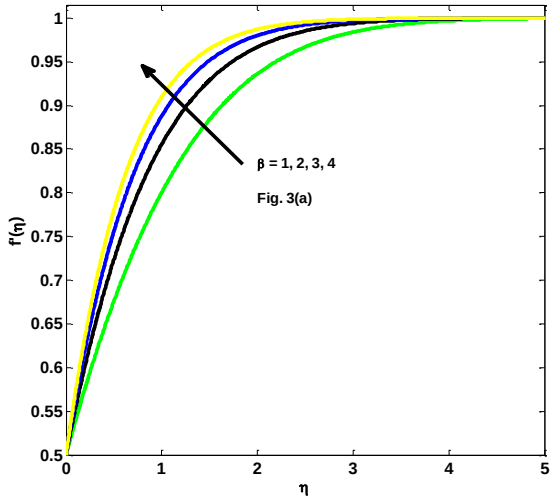


Figure 3(a): $f'(\eta)$ for picked values of $\beta$

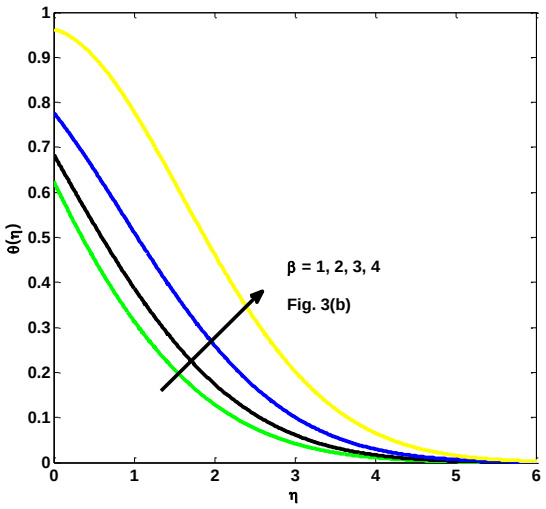


Figure 3(b): $\theta(\eta)$ for picked values of $\beta$

Figure 4 illuminate the effect of different magnetic field parameter $(M)$ values on non-dimensional velocity include the case $M = \mathbf{0}$ of pure hydrodynamic flow means nonexistence of magnetic field. It is shown that the velocity profile decreases with the increasing of $M$ is implies that the momentum boundary layer thickness becomes thinner. Physically, increasing the $M$ values lead to strong Lorentz force along the vertical direction which offers more resistance to the flow.

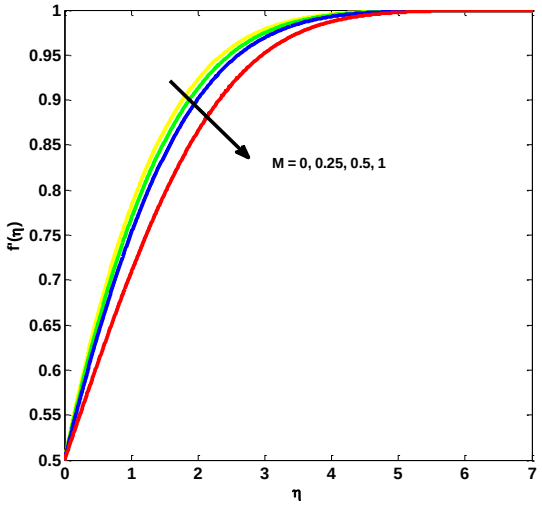


Figure 4: $f'(\eta)$ for picked values of $M$.

The effect of thermal radiation parameter $R$ on the width of temperature profile is explained in the Figure 5 and its stats that enhancing the radiation factor rises the thickness of the thermal boundary layer due to rate of heat transferred to fluid by increased radiation.

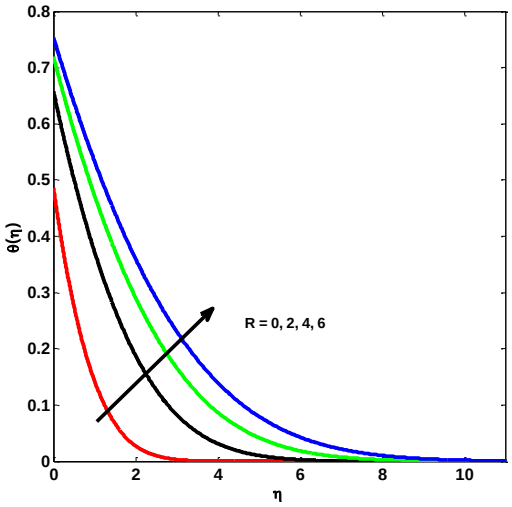


Figure 5: $\boldsymbol{\theta}(\eta)$ for picked values of $R$

The ratio of momentum to thermal diffusivity in the boundary layer is known as Prandtl number and it identifies a desperate thermophysical property of a fluid. From the Figure 6 if the values of $Pr$ rises, the momentum diffusivity is larger than thermal diffusivity which occurs in low-conductivity fluids and as a result, both the thickness of the thermal boundary layer and temperature distribution decline also rise in heat transfer rate.

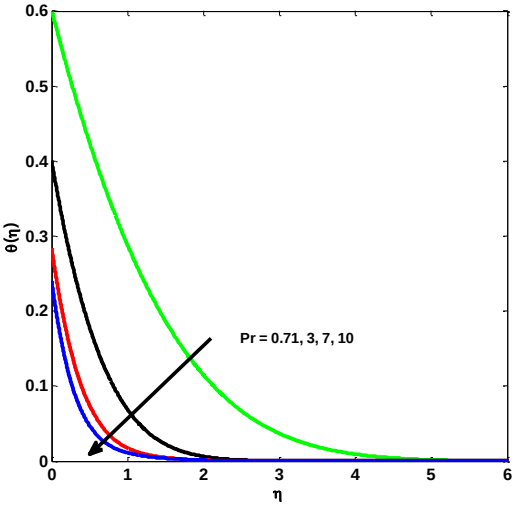


Figure 6: $\boldsymbol{\theta}(\eta)$ for picked values of $Pr$

Figure 7 shows the effect of erratic viscous dissipation parameter $(Ec)$ on temperature

profile. The Eckert number articulate the rapport between the kinetic energy in the flow and the enthalpy, also causes the transformation of kinetic energy into internal energy by the work that is done against the viscous fluid stresses. While increase in Eckert number resulting to increase the kinetic energy which leads to increases the collision of molecules and such increased collision molecules increases the dissipation of heat in the boundary layer region and therefore increases the temperature profile.

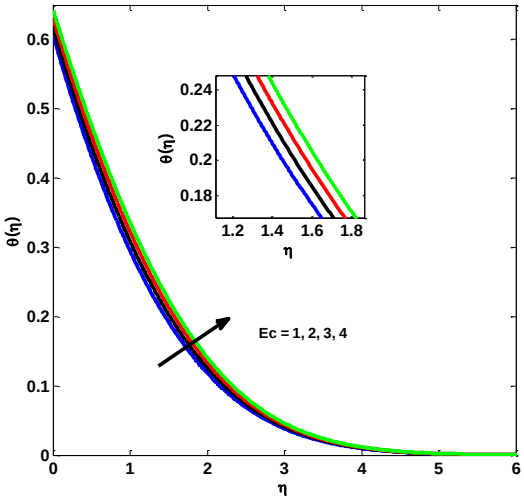


Figure 7: $\theta(\eta)$ for picked values of $Ec$

The heat generation/absorption parameter $Q$ shows the significant effect on the dimensionless temperature profile of the fluid. The presence of external heat source causes to increase in both the temperature distribution and thermal state of the fluid and hence increases the thermal boundary layer thickness. So, the temperature profile increases with an increase in the values of $Q$ which shown in Figure 8.

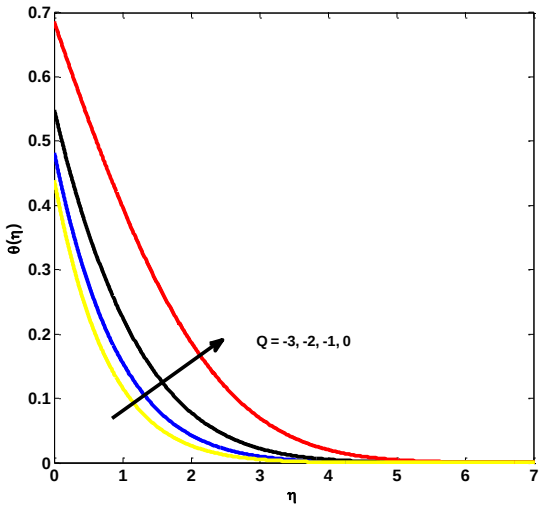


Figure 8: $\theta(\eta)$ for picked values of $Q$

The effect of Schmidt number $(Sc)$ on concentration profile is shown in Figure 9 and which describes decreases nanoparticle volume fraction with an increase in $Sc$. Due to the Schmidt number being the ration of momentum diffusivity to mass diffusivity, an increase in $Sc$ corresponds to the decrease in Brownian diffusion coefficient and higher momentum diffusivity can result in more nanoparticle penetration.

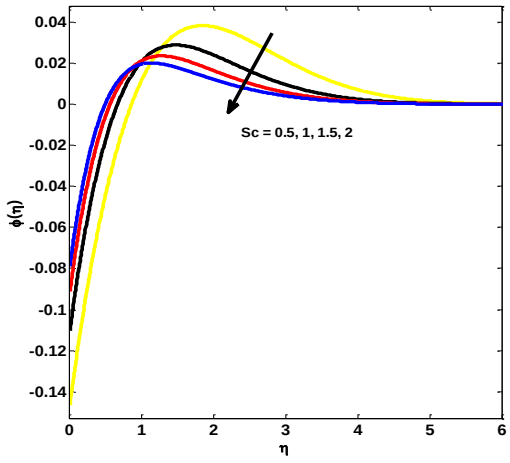


Figure 9: $\theta(\eta)$ for picked values of $Sc$

The impact of thermophoresis on the nanoparticle concentration is depicted in Figure 10. From this we conclude that, when thermophoresis increases, the nanoparticle concentration decreases. Effect of Brownian motion on the nanoparticle concentration is

shown in Figure 11. Here, we can see that, as the Brownian parameter increases, nanoparticle concentration increases throughout the flow domain.

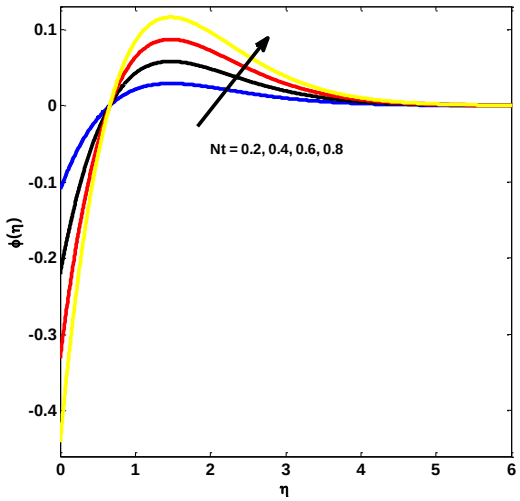


Figure 10: $\boldsymbol{\varphi}(\eta)$ for picked values of $Nt$

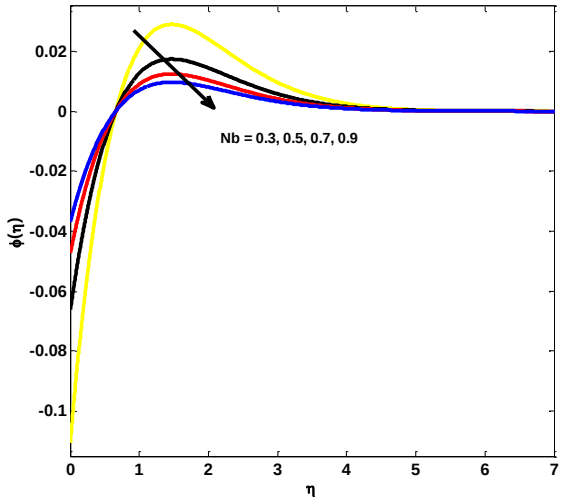


Figure 11: $\theta(\eta)$ for picked values of $Nb$

Effect of chemical reaction parameter (Γ) on nanoparticle volume fraction profile is shown in Figure 12 for different positive values of Γ which reveals that the nanoparticle volume fraction decreases for constructive chemical reaction parameter.

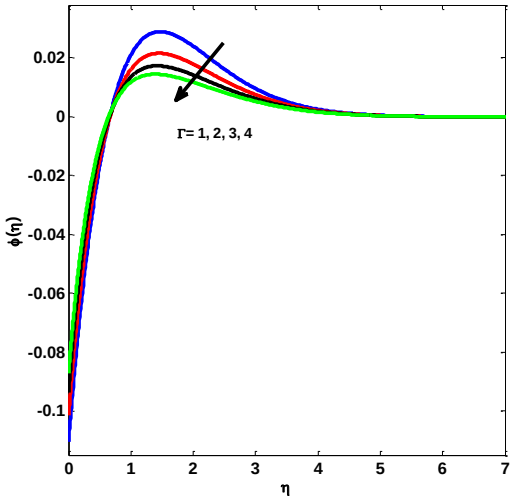


Figure 12: $\theta(\eta)$ for picked values of Γ

The impact of suction parameter on velocity and temperature profile of the nanofluid is depicted via Figure 13(a) and 13(b) respectively and we observed that with enrichment of $s$, the nanofluid velocity increased because of improvement in momentum boundary layer thickness due to enrichment impact of suction parameter $s$ but the decreasing behavior was perceived over the temperature profile because of an upsurge in the rate of heat transfer.

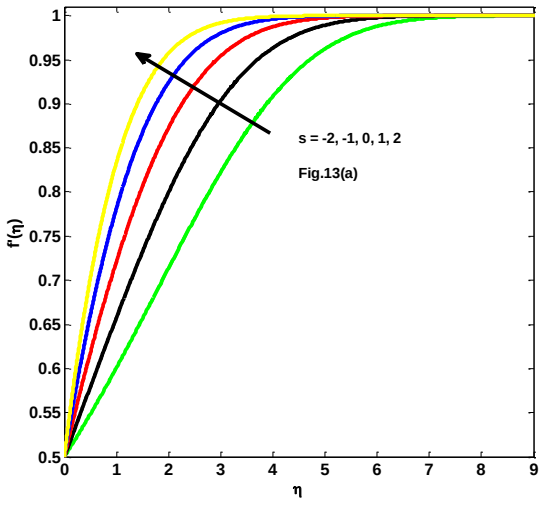


Figure 13(a): $f'(\eta)$ for picked values of $s$

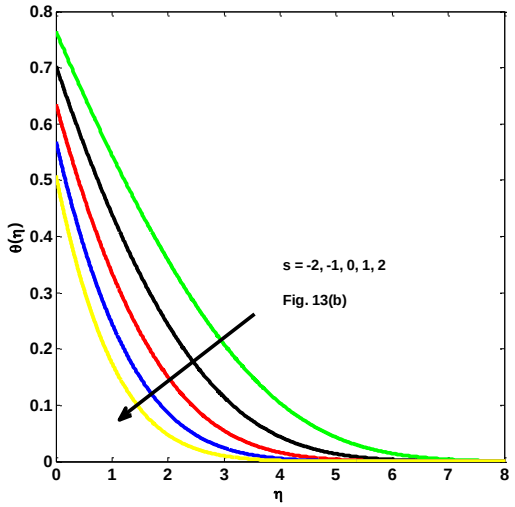


Figure 13(b): $\theta(\eta)$ for picked values of $s$

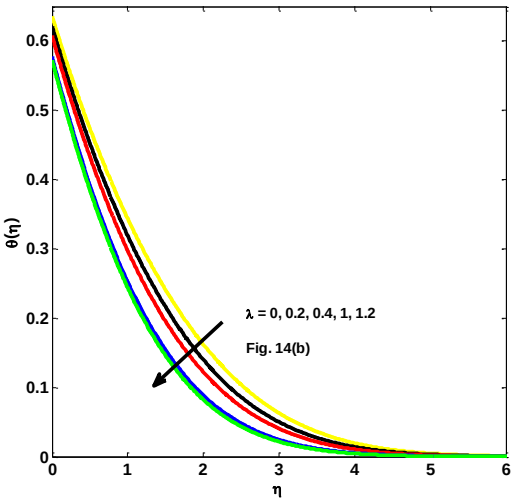


Figure 14(b): $\theta(\eta)$ for picked values of $\lambda$

The influences of velocity ratio parameter on flow velocity, temperature and concentration profiles are revealed through Figures 14(a), 14(b) and 14(c) respectively. As the values of velocity ratio upsurge, the boundary layer thickness rises and the flow has boundary layer structure. The graph of velocity is possible when the free steam velocity is less than or equal to the velocity of stretching sheet. That is when velocity ratio is less than or equal to one. But as the value of velocity ratio parameter increases, thermal boundary layer thickness decreases as well as the same result will reflect on concentration profile of the nanofluid.

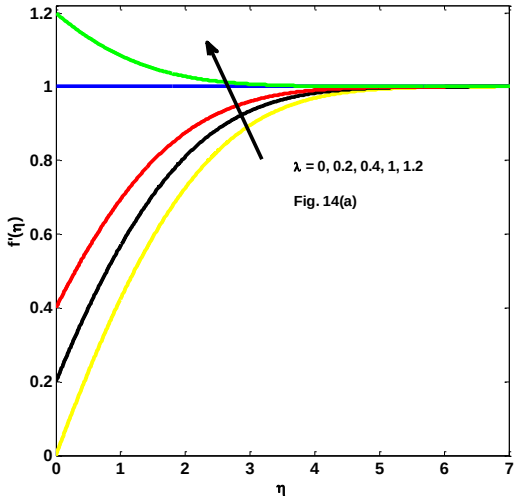


Figure 14(a): $f'(\eta)$ for picked values of $\lambda$

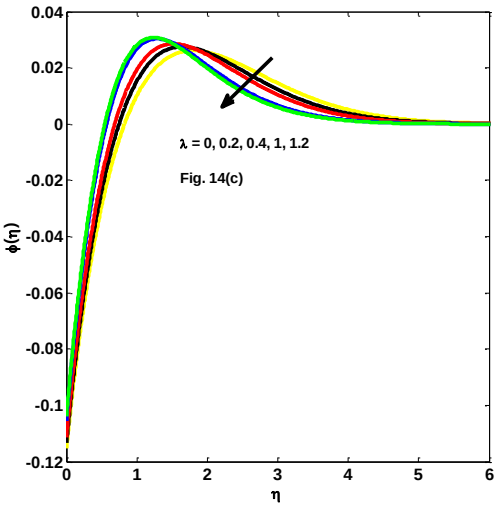


Figure 14(c): $\phi(\eta)$ for picked values of $\lambda$

Figure 15(a) gives the influence of thermal Biot number $(bi)$ on the temperature profile. Due to large Biot number simulates a strong heat convection surface which leads to more heat to the surface and hence the fluid temperature increases with the increment in $bi$. From Figure 15(b) it is observed that increases the fluid concentration effectively with increasing values of $bi$.

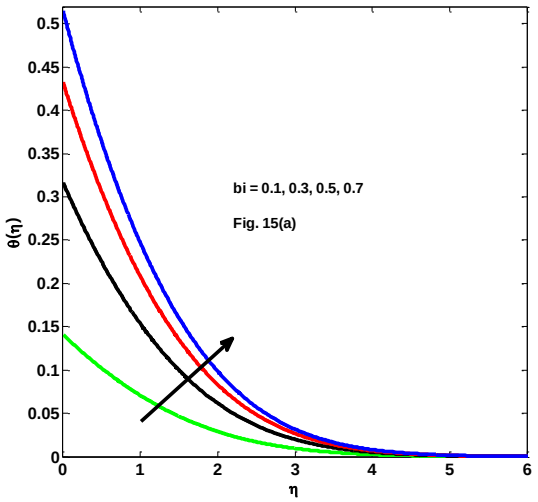


Figure 15(a): $\theta(\eta)$ for picked values of $bi$

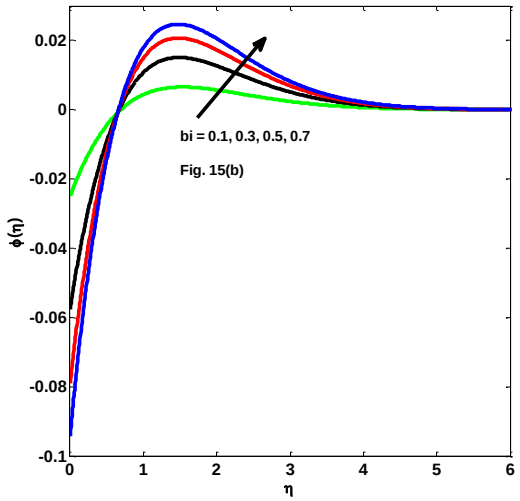


Figure 15(b): $\phi(\eta)$ for picked values of $bi$

The Variation of skin-friction coefficient $\left(\frac{1}{2-\beta}\right)^{1/2} f''(0)$ against Wedge parameter $\beta$ for different values of magnetic parameter $M$, and Casson fluid parameter $\gamma$ reveals in the Figure 16 and it is very clear that the skin-friction coefficient is increased with both the increase of $M, \gamma$ and it also observed that as $\beta$ increases skin-friction coefficient increases. Figure 17 gives the plots of Nussult number $-\theta'(0)$ versus the Eckert number $Ec$ for different values of heat source or sink parameter $Q$ and thermal radiation parameter $R$. It is observed that the Nussult number increases with both the increased values of $Q$ and $R$. In Figure 18 the effect of thermophoresis parameter $Nt$ on Sherwood number $-\varphi'(0)$ is depicted for different values of Brownian motion parameter $Nb$ and Schmidge number $Sc$ and it is clearly explaining that Sherwood number diminishes with both the enhanced values of $Nb$ and $Sc$. It is also observed that Sherwood number increases rapidly for larger values of $Nt$.

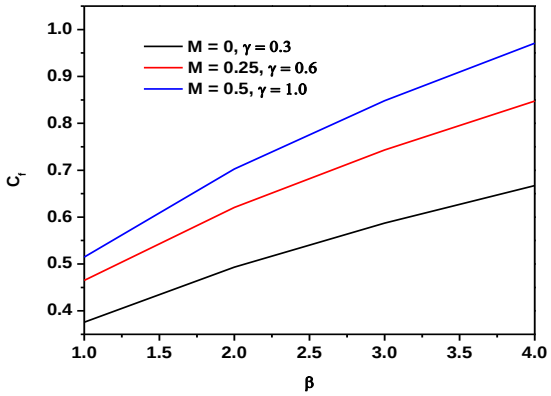


Figure 16: Effect of $M, \gamma$ and $\beta$ on skin friction coefficient

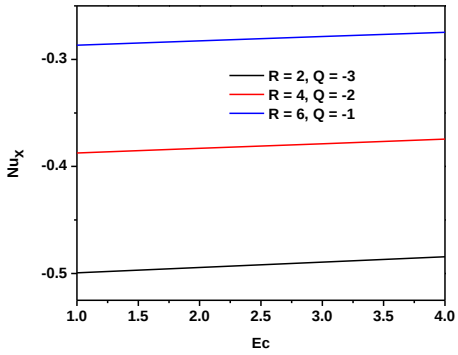


Figure 17: Effect of $R, Q$ and $Ec$ on heat transfer rate

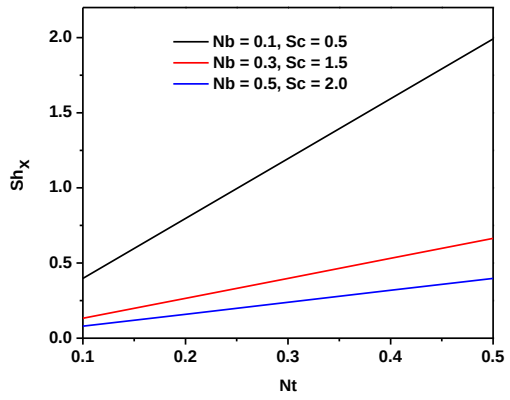


Figure 18: Effect of $Nb, Sc$ and $Nt$ on mass transfer rate

## 5. Conclusion

The present study talks about the analysis of viscous dissipation and radiation effects on MHD heat transfer flow of Casson nanofluid through a moving wedge by incorporating the effects of Brownian and thermophoresis under the convective boundary condition and internal heat absorption/generation. Governing non-linear partial differential equations are turned into non-linear ordinary differential equations by using appropriate similarity transformations. The following specific conclusions have been drawn from above established results.

- The results are confirmed with N. Amar et al, Ahmad et al, Ullah et al, Kuo in good agreement.
- The effect of Casson fluid parameter $\gamma$, wedge parameter $\beta$ enhances the velocity profile whereas magnetic field parameter $M$ reduces the velocity profile.
- Both the velocity ratio parameter $\lambda$ and the suction parameter $s$ augments the velocity profile but these two parameters show the differing effect on temperature profile.
- Temperature distribution increases with increase of thermal radiation $R$, wedge parameter $\beta$ and internal heat absorption $Q$ and decreases with increase of Prandtle number $Pr$ and Schmidge number $Sc$.
- The nanoparticle profile decreases with increase of Brownian motion $Nb$, Schmidge number $Sc$ and chemical reaction parameter $\Gamma$ where as it increase with increase of thermophoresis $Nt$.
- The skin-friction coefficient values increase with all the increase of $M, \gamma$ and $\beta$.
- The rate of heat transfer increases with both the increased values of $Q$ and $R$.
- Sherwood number diminishes with both the enhanced values of $Nb$ and $Sc$ and increases rapidly for larger values of $Nt$.

*References*

[1]. M. A. Kumar, Y. D. Reddy, V. S. Rao, and B. S. Goud, Case Studies in Thermal Engineering, 24: 100826, 2021.
[2]. O. D. Makinde, A. Aziz, International Journal of Therm. Sci., 50:1326, 2011.
[3]. S. Nadeem, R. U. Haq, and C. Lee, Scientia Iranica, 19: 1550, 2012.
[4]. M. G. Reddy, J. Sci. Res., 6: 257, 2014.
[5]. B. S. Goud, Y. D. Reddy, V. S. Rao, and Z. Hayat Khan, Journal of Naval Architecture and Marine Engineering, 7:143, 2020.
[6]. B. S. Goud, Z. H. Khan, and M. Hamid, Heat Transfer, 50: 6129, 2021.
[7]. B. S. Goud, P. P. Kumar, and B. S. Malga, Partial Differential Equations in Applied Mathematics, 2: 100015, 2020.
[8]. S. Nadeem, R.U. Haq, C. Lee, Sci. Iranica B, 19: 1550, 2012.
[9]. T. Hayat, S.A. Shehzad, A. Alsaedi, Appl. Math. Mech., 33: 1301, 2012.
[10]. K. Bhattacharyyaa, T. Hayat, A. Alsaedic, Chin. Phys. B, 22: 024702 2013.
[11]. S. Mukhopadhyay, I. Chandra Mondal, A.J. Chamkha, Heat Transfer Asian Res., 42: 665, 2013.
[12]. S. Nadeem, R.U. Haq, N.S. Akbar, Nonotechnology, 13: 109, 2014.
[13]. R.U. Haq, S. Nadeem, Z.H. Khan, T.G. Okedayo, Cent. Eur. J. Phys., 12: 862, 2014.

[14]. A. Postelnicu, I. Pop, Appl. Math. Comput., 217: 4359, 2011.
[15]. N.G. Kafoussias, N.D. Nanousis, Can. J. Phys., 75:733, 1997.
[16]. S. Mukhopadhyay, I. Chandra Mandal, Chin. Phys. B, 23: 4, 2014.
[17]. N. Kishan, International journal of mathematics and computer applications research, 3:15, 2013.
[18]. N. Kishan, P. Amrutha, International journal of automotive and mechanical engineering, 14: 965, 2009.
[19]. M.A. Hossain, M.S. Munir, D.A.S. Rees, Int. J. Therm. Sci., 39:635, 2000.
[20]. A.J. Chamkha, M.M. Quadri, I. Camille, Heat Mass Transf., 39: 305, 2003.
[21]. A. Pantokratoras, Int. J. Therm. Sci., 45: 378, 2006.
[22]. S. Mukhopadhyay, J. Appl. Fluid. Mech., 2: 29, 2009.
[23]. D. Pal, H. Mondal, Appl. Math. Comput., 212: 194, 2009.
[24]. X. Su, L. Zheng, X. Zhang, J. Zhang, Chem. Eng. Sci., 78:1, 2012.
[25]. M. A. Hossain, S. Bhowmik, and R. S. R. Gorla, Int. J. Eng. Sci., 44: 607, 2006.
[26]. R. K. Deka and S. Sharma, American Journal of Computational and Applied Mathematics, 3: 74, 2013.
[27]. D. Srinivasacharya, U. Mendu, and K. Venumadhav, Procedia Engineering, 127, 1064: 2015.
[28]. M. Veera Krishna, Ali J. Chamkha. Journal of Porous Media, 22(2): 209, 2019.
[29]. M. Veera Krishna, P.V.S. Anand, Ali J. Chamkha. Special Topics & Reviews in Porous Media: An International Journal, 10 (3): 203, 2019.
[30]. M. Veera Krishna, B.V. Swarnalathamma, Ali J. Chamkha. Journal of Ocean Engineering and Science, 4(3): 263, 2019.
[31]. Krishna, M.V., Chamkha, A.J. J Egypt Math Soc., 28 (1): 3826, 2020.
[32]. M. Veera Krishna, Kamboji Jyothi, Ali J. Chamkha, Journal of Porous Media, 23(8): 751, 2020.
[33]. M. Veera Krishna, K. Bharathi, Ali J. Chamkha. Interfacial Phenomena and Heat Transfer, 6(3): 253, 2018.
[34]. S.U.S. Choi, ASME, USA, 66: 99, 1995.
[35]. S. U. S. Choi, Proceedings of the 1995, ASME International Mechanical Engineering Congress and Exposition, 66: 99, 1995.
[36]. M.Y. Malik, M. Naseer, S. Nadeem, A. Rehman, Appl. Nanosci., 4: 869, 2014.
[37]. Rizwan U.l. Haq, S. Nadeem, Z. Hayyat Khan, Toyin Gideon Okedayo, Cent. Eur. J. Phys., 12: 862, 2014.
[38]. M. Madhu, N. Kishan, J. Fluids, ID634186, 2015.
[39]. M. Mustafa, J.A. Khan, AIP Adv., 5: 077148, 2015.
[40]. W. Ibrahim, O.D. Makinde, J. Aerospace Eng., 29: 04015037, 2015.
[41]. A. J. Chamkha, S. Abbasbandy, A. M. Rashad, and K. Vajravelu, Transport in Porous Media, 91: 261, 2012.
[42]. W. A. Khan and I. Pop, Mathematical Problems in Engineering, 2013: 7, (2013).
[43]. A. Mahdy and A. Chamkha, International Journal of Numerical Methods for Heat and Fluid Flow, 28: 2567, 2018.
[44]. N. Amar, N. Kishan, Advances in Mathematics: Scientific Journal, 10 (3): 1357, 2021.
[45]. Jamal Shah, Farhad Ali, Naveed Khan, Zubair Ahmad, Saqib Murtaza, Ilyas Khan, Omar Mahmoud, Sci Rep., 12: 17364, 2022.
[46]. Asad Ullah, Ramadan A. Zein Eldin, Hamiden Abd El-Wahed Khalifa, ACS Omega, 8(12): 10991, 2023.
[47]. Ragulkumar, E., Palani, G., Sambath, P. Sci Rep., 13: 2878, 2023.
[48]. Y. Suresh Kumar, Shaik Hussain, K. Raghunath, Farhan Ali, Kamel Guedri, Sayed M. Eldin, M. Ijaz Khan. Sci Rep., 13: 4021, 2023.

[49]. G. N. Amar, N.Kishan, B. Shankar Goud, J. Nanofluids, 12(3): 643, 2023.
[50]. Macha Madhu and Naikoti Kishan, Mechanics & Industry, 18: 210, 2017.
[51]. Rossenald s, Astrophysik und atom-theoretische Grundlagen, Berlin:Springer, 1931.
[52]. K.Ahmad,Z.Hanouf,andA.Ishak,Eur.Phys .J.Plus,132: 1, 2017.
[53]. I. Ullah, S. Shafie, I. Khan, Malaysian Journal of Fundamental and Applied Sciences, 13: 637, 2017.
[54]. B. L.Kuo,Acta Mechanica, 164: 161, 2003.

**Contribution of Individual Authors to the Creation of a Scientific Article (Ghostwriting Policy)**

The authors equally contributed in the present research, at all stages from the formulation of the problem to the final findings and solution.

**Sources of Funding for Research Presented in a Scientific Article or Scientific Article Itself**

No funding was received for conducting this study.

**Conflict of Interest**

The authors have no conflicts of interest to declare that are relevant to the content of this article.